# Detailed Magnetic Behavior of Nickel Near its Curie Point

JAMES S. KOUVEL
*General Electric Research Laboratory, Schenectady, New York*

AND

MICHAEL E. FISHER*
*The Rockefeller Institute, New York, New York*

(Received 15 July 1964)

The temperature dependence of the initial susceptibility $\chi_0$ of nickel above the Curie point $T_c$ and the field dependence of its magnetization at $T_c$ are deduced from the data of Weiss and Forrer and found to be at variance with the simple molecular-field model. Instead, the experimental $\chi_0^{-1}$-versus-$T$ curve just above $T_c$ is shown to follow the simple relation $\chi_0^{-1}=A\,(T-T_c]^\gamma$, with $\gamma=1.35\pm0.02$, in excellent agreement with the $\frac{4}{3}$-power relation recently predicted from the exact series for the Heisenberg model. From the coefficient $A$, it is deduced that $\mu_0$, the average atomic moment, is 0.642 $\mu_B$ and that the individual electron moments are in a state corresponding to $S=\frac{1}{2}$. At higher temperatures, the $\chi_0^{-1}$-versus-$T$ curve deviates from the Heisenberg-model predictions, possibly because of a gradual rise in $\mu_0$ with increasing temperature. Up to the highest field $H$ of measurement, the magnetization at $T_c$ is shown to vary as $H^\epsilon$ with $\epsilon=0.237$, which is consistent with the exponent values for an analogous empirical relationship between the density and pressure of several different gases at their critical points.

## INTRODUCTION

CONSIDERABLE attention has been given recently to the Ising and Heisenberg models of a ferromagnet, particularly to the behavior near the critical temperature. Especially noteworthy are the accurate expressions for the initial susceptibility ($\chi_0$) just above the Curie point ($T_c$), which have been derived by two different methods based on power series expansions. By studying the ratios of successive terms in the power series, Domb and Sykes found for the three-dimensional Ising[1] and Heisenberg[2] models that, as $T$ approaches $T_c$,

$$\chi_0^{-1} \propto (T-T_c)^\gamma, \qquad (1)$$

and that to a very close approximation the exponent $\gamma$ is 5/4 in the Ising case and $\frac{4}{3}$ in the Heisenberg case. This $\chi_0^{-1}$-versus-$T$ relationship, with essentially the same values for $\gamma$, was also obtained by the method of Padé approximants and reported by Baker[3a] for the Ising model and by Gammel *et al.*[4] for the Heisenberg model. The latter method was also recently applied to the Heisenberg ferromagnet by Baker with broadly similar results.[3b] It was found[2,4] that $\gamma=\frac{4}{3}$ was appropriate for all three cubic lattices: fcc, bcc, and sc; moreover, this $\gamma$ value was found to obtain for all (half-integral) values of the spin quantum number $S$. Indeed, it is only through the proportionality factor between the right- and left-hand sides that Eq. (1) was found to vary with crystal-structure type[4] and value of $S$.[2,4]

For the case of $\gamma=1$, Eq. (1) is identical with the familiar Curie-Weiss relationship deduced from molecular-field theory. Hence, if susceptibility measurements on some ferromagnetic material were to reveal a $\gamma$ value decidedly closer to $\frac{4}{3}$ (or 5/4) than to unity, such a result would strongly imply the existence of the short-range correlations in spin orientation that are taken into account in the Heisenberg (and Ising) model but not in the molecular field model. Pertinent to this, Noakes and Arrott[5] have recently made some very careful measurements of the initial susceptibilities of iron and some iron-vanadium alloys just above their Curie points. Very small applied fields (25 to 100 Oe) were used in these experiments in order that the measured susceptibilities truly represent those in vanishingly small fields. Comparing their $\chi_0$-versus-$T$ data for iron with Eq. (1), Noakes and Arrott were able to obtain an excellent fit with $\gamma=1.37$ ($\pm0.04$). Their data for the alloys also gave good agreement with Eq. (1), except that the value deduced for $\gamma$ decreased progressively with increasing vanadium concentration, reaching 1.24 at one percent. It should also be mentioned that the initial susceptibilities of the ferromagnetic salts $CuK_2Cl\cdot 2H_2O$ and $Cu(NH_4)_2Cl_4\cdot 2H_2O$ are fitted quite well from about 4% above $T_c$ to about 50% above $T_c$ by Eq. (1) with $\gamma=1.36$ and 1.37, respectively.[6]

The close correspondence between these susceptibility results and the recent Heisenberg model calculations cited above is particularly remarkable in the case of iron, since the long-range exchange forces in a ferromagnetic metal would appear to preclude any significant comparison with a model in which only nearest-neighbor interactions are considered explicitly. The imperfect localization of moment in a ferromagnetic metal would also argue against the application of a Heisenberg model. Nevertheless, the agreement between the Noakes and Arrott results for iron, and Eq. (1) with $\gamma\approx\frac{4}{3}$,

* On leave for 1963–64 from The Wheatstone Physics Laboratory, King's College, London, England.

[1] C. Domb and M. F. Sykes, J. Math. Phys. **2**, 63 (1961).

[2] C. Domb and M. F. Sykes, Phys. Rev. **128**, 168 (1962).

[3] (a) G. A. Baker, Phys. Rev. **124**, 768 (1961); (b) **129**, 99 (1963).

[4] J. Gammel, W. Marshall, and L. Morgan, Proc. Roy. Soc. (London) **A275**, 257 (1963).

[5] J. E. Noakes and A. Arrott, J. Appl. Phys. **35**, 931 (1964).

[6] A. R. Miedema, H. Van Kempen, and W. J. Huiskamp, Physica **29**, 1266 (1963).

cannot be summarily dismissed as fortuitous, since it is quite possible that the rigorously correct model for a ferromagnetic metal would predict a susceptibility behavior near the Curie point that is similar to that predicted by the rigorous Heisenberg model, even though these models may diverge in their statements about other magnetic properties. For this reason, we felt encouraged to examine the case of nickel, whose detailed magnetic behavior near the Curie point has been previously measured and found to be anomalous with respect to the molecular-field theory.

## ANALYSIS AND DISCUSSION

In this re-examination of the magnetic behavior of nickel, we have relied almost entirely on the data of Weiss and Forrer[7] since they give the most comprehensive and reliable magnetization-field-temperature information in the immediate vicinity of the Curie point (~630°K). Some of this information is presented in Fig. 1 in the form of isotherms of $\sigma$, the magnetization per gram, versus $H$, the internal field (the applied field corrected for demagnetization). Although these curves clearly indicate a gradual transition between ferromagnetism and paramagnetism, their curvature at low fields makes it very difficult to extract accurate values for the initial susceptibility $\chi_0$ (i.e., $d\sigma/dH$ at $H=0$) above the Curie point. Indeed, it is hard to know precisely where the Curie point is on the basis of these curves. We have therefore resorted to the useful

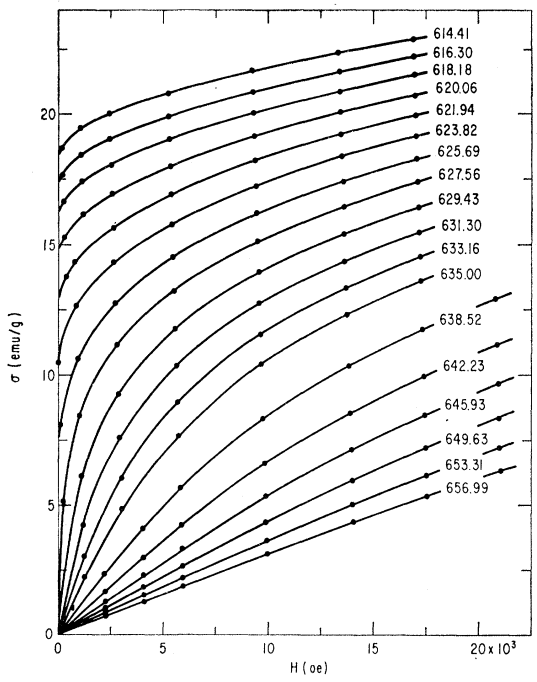


FIG. 1. Magnetization versus internal field for nickel at different temperatures, from data of Weiss and Forrer.[7]

[7] P. Weiss and R. Forrer, Ann. Phys. (Paris) 5, 153 (1926).

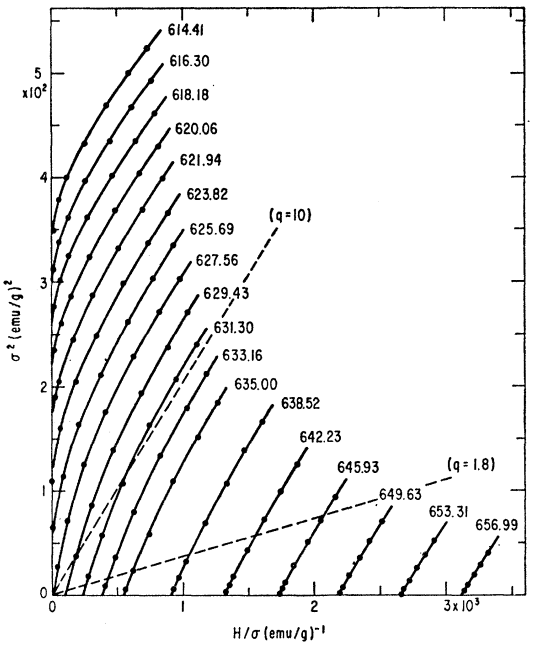


FIG. 2. Data of Fig. 1 plotted as isotherms of $\sigma^2$ versus $H/\sigma$; dashed lines calculated from Eq. (2) for different $q$.

technique first proposed by Belov and Goryaga,[8] and later independently by one of us,[9] of plotting the data at various temperatures as $\sigma^2$ versus $H/\sigma$. The nickel data are plotted in this way in Fig. 2, and, as we show, the curves in this figure are much more amenable to systematic analysis than those in Fig. 1.

A brief description at this point of the molecular-field theory basis for the $\sigma^2$ versus $H/\sigma$ technique provides a convenient frame of reference for our detailed discussion of the nickel data. We therefore consider a system of atomic moments each of magnitude $\mu_0$, whose energy spectrum in a total effective field $H_{\text{eff}}$ consists of $2S+1$ levels with a separation of $\mu_0 H_{\text{eff}}$. It should be noted that $S$, the half-integral spin quantum number, is *not* necessarily to be identified in a metal such as nickel with $\mu_0/g\mu_B$, $g$ being the spectroscopic splitting factor and $\mu_B$ the Bohr magneton. The magnetization (per gram) is expressed by the usual Brillouin function as follows:

$$\sigma/\sigma_0 = B_S(x), \quad x \equiv \mu_0 H_{\text{eff}}/kT,$$

where $\sigma_0$ is the magnetization corresponding to complete ferromagnetic alignment and thus equals $N\mu_0$, $N$ being the number of atoms per gram. The exchange coupling between the moments is represented by $\lambda\sigma$, an average molecular field proportional to the magnetization; hence, $H_{\text{eff}}=\lambda\sigma+H$, where $H$ is the applied field corrected for demagnetization. If $B_S(x)$ is expanded as a power series in $x$ which is then reverted into a power

[8] K. P. Belov and A. N. Goryaga, Fiz. Met. Metallov. 2, No. 1, 3 (1956).

[9] J. S. Kouvel, General Electric Res. Lab. Rept. No. 57-RL-1799 (1957), unpublished.

series in $\sigma/\sigma_0$, it is found that

$$x\equiv\mu_0(H+\lambda\sigma)/kT=a(\sigma/\sigma_0)+b(\sigma/\sigma_0)^3+\cdots,$$

where

$$a\equiv 3S/(S+1),\quad b\equiv\{9S/10(S+1)\}\{1+S^2/(S+1)^2\}.$$

Since $\sigma\rightarrow 0$ at $H=0$ as $T$ increases toward the Curie point $T_c$, it follows that $\mu_0\lambda/kT_c=a/\sigma_0$. Substituting this into the above and eliminating $\lambda$, we obtain

$$H=(T-T_c)\sigma/C+(kT/q\mu_B)(\sigma/\sigma_0)^3+\cdots, \quad (2a)$$

$$C\equiv Np^2\mu_B^2/3k, \quad (2b)$$

$$p\equiv n_0\{(S+1)/S\}^{1/2},\quad (n_0\equiv\mu_0/\mu_B), \quad (2c)$$

$$q\equiv 10n_0(S+1)/9S\{1+S^2/(S+1)^2\}, \quad (2d)$$

where $C$ is the familiar Curie constant, $p$ and $n_0$ are the effective paramagnetic and ferromagnetic moments (in $\mu_B$), respectively, and $q$ may be thought of as still another kind of effective moment (also in $\mu_B$). Near $T_c$, $\sigma/\sigma_0\ll 1$ in all but extremely high fields, and the terms of higher order in $\sigma/\sigma_0$ than those shown in Eq. (2a) can be neglected. Then according to this equation, curves of $\sigma^2$ versus $H/\sigma$ at various temperatures near $T_c$ should form a progression of essentially parallel straight lines, the one for $T=T_c$ passing through the origin. Moreover, the intersections of these curves for $T>T_c$ with the $H/\sigma$ axis give values for $\chi_0^{-1}$, which according to Eq. (2a) should vary with temperature as prescribed by the Curie-Weiss relation

$$\chi_0^{-1}\equiv(H/\sigma)_{\sigma\rightarrow 0}=(T-T_c)/C \quad (3)$$

and should go to zero at $T=T_c$. The $\sigma^2$-versus-$H/\sigma$ plot has therefore been proposed[8,9] as a convenient method for determining the Curie point of a ferromagnet; an analogous method based on a $\sigma^3$-versus-$H$ plot has also been recommended.[10]

Even though the $\sigma^2$-versus-$H/\sigma$ curves for nickel shown in Fig. 2 deviate from the straight lines predicted from the molecular-field theory (a discrepancy we shall presently discuss), it is nevertheless clear that the curves for 627.56°K and above can be extended smoothly and unambiguously into the $H/\sigma$ axis to give reliable values for $\chi_0^{-1}$. This is also true for the Weiss and Forrer data at temperatures well above those represented in Fig. 2. The $\chi_0^{-1}$ values thus determined are plotted against temperature (up to about 720°K) in Fig. 3, and it is immediately evident that the smooth curve drawn through all the points does not follow the linear relation of Eq. (3). According to the Weiss and Forrer data at higher temperatures, the concave-upward curvature in $\chi_0^{-1}$-versus-$T$ persists up to about 800°K, above which the curve straightens out and is linear at the maximum temperature of about 900°K. Subsequent susceptibility measurements on nickel from about 700 to 1500°K by Sucksmith and Pierce[11] have confirmed these results and have shown that above a linear region from about 800 to 1100°K the $\chi_0^{-1}$-versus-$T$ curve has a small but distinct concave-downward curvature. Both sets of results indicated that an extrapolation of the linear portion of the $\chi_0^{-1}$-versus-$T$ curve intersects the $T$ axis at 650°K, and that the slope of this extrapolated curve (shown as a dashed line in Fig. 3) corresponds to a value for the effective paramagnetic moment $p$ of 1.61. If we consider the values for $p/n_0$ determined from Eq. (2c) and listed in Table I for different $S$ and take $n_0=0.606$ from the saturation moment at 0°K, we obtain values for $p$ (also listed in Table I) that are all considerably

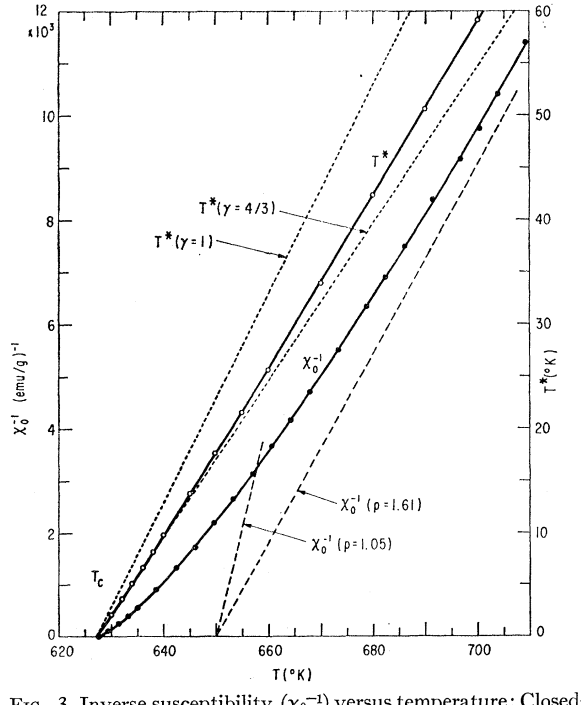


FIG. 3. Inverse susceptibility ($\chi_0^{-1}$) versus temperature: Closed-circled points derived from nickel data of Weiss and Forrer[7]; dashed lines calculated from Eq. (3) for different $p$. $T^*$ versus $T$: Open-circled points derived from experimental $\chi_0^{-1}$-versus-$T$ curve and Eq. (4); dotted lines calculated from $T^*=(T-T_c)/\gamma$ for different $\gamma$.

TABLE I. Values of $p/n_0$ and $q/n_0$ computed from Eqs. (2c) and (2d) for different $S$, and corresponding values of $p$ and $q$ (effective moments in $\mu_B$) for $n_0$ (ferromagnetic moment in $\mu_B$) = 0.606. Also, values of $p$ and $n_0$ for nickel at $T_c$ obtained from curves in Fig. 5.

| $S$ | $\frac{1}{2}$ | 1 | $\infty$ |
|---|---|---|---|
| $p/n_0$ | $\sqrt{3}$ | $\sqrt{2}$ | 1 |
| $p$ ($n_0=0.606$) | 1.050 | 0.857 | 0.606 |
| $q/n_0$ | 3 | 16/9 | 5/9 |
| $q$ ($n_0=0.606$) | 1.818 | 1.077 | 0.337 |
| $p$ ($T=T_c$) | 1.112 | 1.194 | 1.283 |
| $n_0$ ($T=T_c$) | 0.642 | 0.844 | 1.283 |

[10] A. Arrott, Phys. Rev. **108**, 1394 (1957).
[11] W. Sucksmith and R. R. Pierce, Proc. Roy. Soc. (London) **A167**, 189 (1938).

smaller than 1.61. Using the calculated $p$ value closest to 1.61 (i.e., 1.05 for $S=\frac{1}{2}$) in conjunction with Eqs. (2b) and (3), we compute a linear $\chi_0^{-1}$-versus-$T$ curve (shown dashed in Fig. 3) which bears little resemblance to the experimental curve.

In an analogous comparison of the experimental $\sigma^2$-versus-$H/\sigma$ curves of Fig. 2 with the predictions of the molecular-field theory, we first note that all these curves have approximately the same slope at the highest fields. In particular, if we consider the curves near the Curie point and match their slope at high fields with that of a straight line (shown dashed in the figure), we find from Eq. (2a), assuming $\sigma_0=57.5$ emu/g (equivalent to $n_0=0.606$), that this line corresponds to a value of $q$ of about 10. Using the values of $q/n_0$ for different $S$ derived from Eq. (2d) and listed in Table I and again taking $n_0=0.606$, we obtain the values for $q$ also listed in the table, which clearly are very much smaller than 10. Equivalently, the calculated $q$ value closest to 10 (i.e., $\sim 1.8$ for $S=\frac{1}{2}$) gives a $\sigma^2$-versus-$H/\sigma$ curve (shown dashed in Fig. 2) which is in striking contrast with the experimental curves.

By having thus established that the $\sigma^2$-versus-$H/\sigma$ curves, as well as the $\chi_0^{-1}$-versus-$T$ curve, for nickel near its Curie point are qualitatively and quantitatively in serious disagreement with the predictions of the molecular-field theory, we have further demonstrated the need for a better theoretical model. The anomalous $\chi_0^{-1}$-versus-$T$ behavior of nickel and similar anomalies in iron and cobalt[12] have long been appreciated and have received considerable theoretical attention. Notable among the models that have dealt explicitly with this problem are Néel's fluctuation model,[13] in which short-range effects manifested as fluctuations in the local magnetization were included in a molecular-field treatment, and Stoner's collective electron model,[14] a simple energy-band treatment in which short-range correlation effects were neglected. Although they represent completely different departures from the simple molecular-field approach, both these models predict $\chi_0^{-1}$-versus-$T$ curves that are concave upward and by suitable parameter adjustment have been made to fit the experimental curve for nickel. However, in neither case was the comparison with experiment extended down to temperatures immediately above $T_c$, where the theoretical $\chi_0^{-1}$-versus-$T$ curves retain a fairly large slope but where the experimental curve in Fig. 3 appears to approach the $T$ axis horizontally. This situation also obtains qualitatively for the $\chi_0^{-1}$-versus-$T$ expression derived by Weiss[15] from a Bethe-Peierls treatment of magnetic short-range order and that derived by Zehler[16] from an Opechowski-Kramers treatment of the Heisenberg localized-moment model. Subsequently, however, using the statistical "spherical model" approach, Lax[17] obtained a $\chi_0^{-1}$-versus-$T$ relationship that reduces near $T_c$ to Eq. (1) with $\gamma=2$ and therefore describes a curve intersecting the $T$ axis with zero slope. This particular point of similarity with the experimental curve for nickel is also satisfied, of course, by the more recent and exact calculations for the Ising and Heisenberg ferromagnets, which were described earlier as giving Eq. (1) with $\gamma=5/4$ and $\frac{4}{3}$, respectively, for $\chi_0^{-1}$-versus-$T$ near $T_c$. Hence, since the $\chi_0^{-1}$-versus-$T$ curve for nickel in Fig. 3 is so well defined by the experimentally derived points even immediately above the Curie point, we decided to compare it in detail with these recent theoretical results.

Reserving the more exact expressions for the temperature dependence of the paramagnetic susceptibility for later discussion, we first test the behavior of nickel near its Curie point against the simple relationship given in Eq. (1). Specifically, consider the function $T^*$ defined by

$$T^*(T)=1/(d/dT)\ln(\chi_0^{-1}) \\ =1/\chi_0(d\chi_0^{-1}/dT). \tag{4}$$

As $T$ approaches $T_c$ this should approach the linear function $(T-T_c)/\gamma$, if Eq. (1) is valid. From the $\chi_0^{-1}$-versus-$T$ curve in Fig. 3 we determine the values of $\chi_0^{-1}$ and $d\chi_0^{-1}/dT$ at various temperatures and from Eq. (4) the corresponding values of $T^*$; these are all listed in Table II. The values of $T^*(T)$ are also plotted in Fig. 3 (open circles), and it is observed that the curve through these points is almost linear and intersects the $T$ axis unambiguously at 627.2°K, which we hereinafter regard as a reliable value for the true Curie temperature. Moreover, from the theoretical limiting $T^*(T)$ curves for $\gamma=1$ and $\gamma=\frac{4}{3}$ shown in the figure

TABLE II. Values of $\chi_0^{-1}$ and $d\chi_0^{-1}/dT$ obtained at different temperatures from experimental $\chi_0^{-1}$-vs-$T$ curve for nickel in Fig. 3, and corresponding values of $T^*$ and $\gamma^*$ computed from Eqs. (4) and (5).

| $T$ (°K) | $\chi_0^{-1}$ [a] | $d\chi_0^{-1}/dT$ [a] | $T^*$ (°K) | $\gamma^*$ |
|---|---|---|---|---|
| 630 | 142 | $68._5$ | $2.0_7$ | $1.35_1$ |
| 632 | 291 | $81._0$ | $3.5_9$ | $1.33_6$ |
| 634 | 460 | $90._0$ | $5.1_1$ | $1.33_0$ |
| 636 | 650 | $97._5$ | $6.6_7$ | $1.32_0$ |
| 638 | 850 | $103._5$ | $8.2_1$ | $1.31_5$ |
| 640 | 1060 | $108._0$ | $9.8_2$ | $1.30_4$ |
| 645 | 1630 | $118._5$ | 13.8 | $1.29_4$ |
| 650 | 2240 | $127._0$ | 17.6 | $1.29_3$ |
| 655 | 2890 | $134._0$ | 21.6 | $1.28_9$ |
| 660 | 3570 | $139._0$ | 25.7 | $1.27_7$ |
| 670 | 5020 | $148._0$ | 33.9 | $1.26_2$ |
| 680 | 6550 | $154._5$ | 42.4 | $1.24_6$ |
| 690 | 8120 | $160._5$ | 50.6 | $1.24_1$ |
| 700 | 9770 | $165._5$ | 59.0 | $1.23_3$ |

[a] $\chi_0$ in emu/g.

[12] See discussion in L. F. Bates, *Modern Magnetism* (Cambridge University Press, London, 1951), 3rd ed., pp. 304, 305.
[13] L. Néel, J. Phys. Radium **5**, 104 (1934).
[14] E. C. Stoner, Proc. Roy. Soc. (London) **A165**, 372 (1938); **A169**, 339 (1939).
[15] P. R. Weiss, Phys. Rev. **74**, 1493 (1948).
[16] V. Zehler, Z. Naturforsch. **5**, 344 (1950).
[17] M. Lax, Phys. Rev. **97**, 629 (1955).

(dotted lines), it is evident that the experimentally derived curve is described just above the Curie point by a value of $\gamma$ very close to $\frac{4}{3}$. As the temperature increases, the experimental values of $T^*$ deviate slowly from the limiting line for $\gamma=\frac{4}{3}$ and may be described by a slowly decreasing effective exponent $\gamma^*$, defined formally by

$$\gamma^*(T)=(T-T_c)/T^* \\ =(T-T_c)(d/dT)\ln(\chi_0^{-1}). \tag{5}$$

As $T$ approaches $T_c$, the function $\gamma^*(T)$ should approach the value $\gamma$. The values of $\gamma^*(T)$ thus derived from $T^*(T)$ are listed in Table II and plotted against temperature in Fig. 4. In this figure we have indicated the maximum error associated with the determination of each $\gamma^*$ value and the most probable curve which gives $\gamma^*(T_c)=\gamma=1.35\pm0.02$. Thus, within the experimental and computational errors, the susceptibility behavior of nickel just above its Curie point agrees almost perfectly with the recent theoretical results of Domb and Sykes[2] and of Gammel *et al.*[4] for the Heisenberg ferromagnet.

We were therefore encouraged to pursue our analysis further and compare some of the information derived from the nickel data (e.g., the decrease of $\gamma^*$ with increasing temperature indicated in Fig. 4) with the more detailed results of the recent Heisenberg-model calculations. The complete closed-form expression obtained by Gammel *et al.* for the paramagnetic susceptibility of a Heisenberg ferromagnet, valid at all temperatures above the Curie point, may be written as

$$\chi_0^{-1}=C^{-1}T(1-\tau)^{4/3}f(\tau), \\ \tau\equiv T_c/T, \\ f(\tau)\equiv\{(1-b_1\tau)(1-b_2\tau)/(1-a_1\tau)(1-a_2\tau)(1-a_3\tau)\}^{4/3}, \tag{6}$$

where $C$ is still the Curie constant defined in Eq. (2). The $a$'s and $b$'s in the expression for $f(\tau)$ [the reciprocals respectively of the $A$'s and $B$'s in Eq. (14) of Ref. 4] are numerical constants that depend only on the crystal structure and the spin quantum number $S$. In all cases, including those in which some of these constants are complex conjugate pairs, $f(\tau)$ is a slowly varying function of $\tau$ over the entire paramagnetic temperature range. Hence, in the immediate vicinity of the Curie point (i.e., for $\tau\approx1$) Eq. (6) reduces to Eq. (1) with $\gamma=\frac{4}{3}$, or more specifically to $\chi_0^{-1}=A(T-T_c)^{4/3}$, where $A\equiv C^{-1}T_c^{-1/3}f(1)$. At the other extreme of very high temperatures (i.e., as $\tau\to0$), Eq. (6) approaches the Curie-Weiss relationship, $\chi_0^{-1}=C^{-1}(T-\theta)$, where $\theta$, the "asymptotic" Curie point, is in general larger than $T_c$. If the function $\gamma^*(T)$ is determined from Eq. (6) by the operations prescribed in Eqs. (4) and (5), it is found in all cases that its value is $\frac{4}{3}$ at $T_c$ and decreases to unity at very high temperatures. By this method, using values for the $a$'s and $b$'s in Eq. (6) appropriate

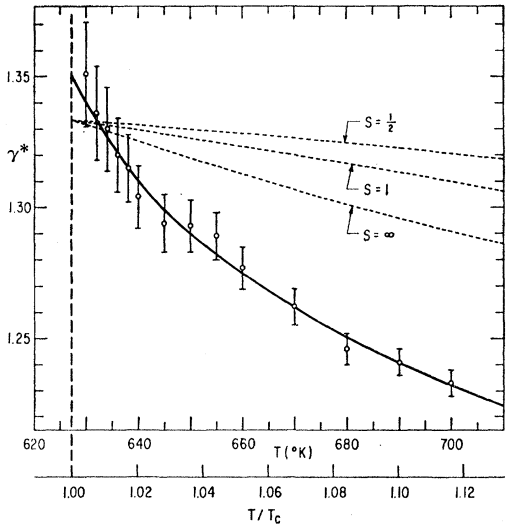


FIG. 4. Temperature dependence of $\gamma^*$: Circled points derived from $T^*$ values in Table II and Eq. (5); dotted curves calculated from Eqs. (5) and (6) for different $S$.

for a fcc structure and for the cases $S=\frac{1}{2}$, 1, and $\infty$, we have computed the $\gamma^*$-versus-$T$ curves shown dotted in Fig. 4, which we can now compare directly with the solid curve derived by the same method from the experimental data on nickel. Although all three of the theoretical curves in this figure show a monotonic decrease of $\gamma^*$ with increasing temperature, none of them can account for more than a minor part of the variation of $\gamma^*$ exhibited by the experimental curve. This discrepancy between the theoretical and experimental $\gamma^*$-versus-$T$ curves can simply mean, of course, that Eq. (6) is inapplicable to nickel, except very close to the Curie point, because of, for example, the neglect of interactions of longer range or the nonlocal character of the spins. However, it is also possible that this discrepancy is caused by a variation with temperature (explicitly or implicitly through thermal expansion) of some of the intrinsic magnetic characteristics of nickel, such as the strength of the exchange coupling and the magnitude of the effective atomic moment, which are represented in Eq. (6) by the fixed constants $T_c$ and $C$, respectively.

To study the consequences of the latter hypothesis, particularly in relation to the magnitude of the atomic moment of nickel at the Curie point, we hold $T_c$ constant in Eq. (6) but regard the effective moment (and hence the parameter $C$) as a temperature-dependent function. We can evaluate $C$ by comparing the experimental and theoretical results according to

$$C=(C\chi_0^{-1})_{\text{theor}}/(\chi_0^{-1})_{\text{exp}}. \tag{7}$$

For $(\chi_0^{-1})_{\text{exp}}$, we take the values listed in Table II; for the same temperatures we compute $(C\chi_0^{-1})_{\text{theor}}$ as defined in Eq. (6), again using the values for the $a$'s

and $b$'s for a fcc structure and $S=\frac{1}{2}$, 1, and $\infty$. The values of $C$ thus obtained are then converted by means of Eq. (2b) into values of $p$, the effective paramagnetic moment (in $\mu_B$ per atom). The latter are plotted against temperature in Fig. 5, and it is evident that regardless of the choice of $S$ there is a slow but irrevocable rise in $p$ with increasing temperature, amounting to an increase of about 5% over the temperature range shown. According to our previous discussion, this increase in $p$ is equivalent to the divergence of the experimental and theoretical $\gamma^*$-versus-$T$ curves in Fig. 4 and may be taken as a possible explanation for the deviation of the susceptibility behavior of nickel from that predicted theoretically in Eq. (6).

Extending the curves in Fig. 5 down to the Curie point, we obtain the values for $p$ listed in Table I. We then apply the appropriate $p/n_0$ ratio given in Table I and transform each of the $p$ values into a value for $n_0$; the $n_0$ values thus obtained for different $S$ are also listed in Table I. Since $n_0$ as defined corresponds to the true atomic moment (in $\mu_B$), it is immediately noted that its Curie-temperature value of 0.642 for $S=\frac{1}{2}$ compares very closely with the value of 0.606 deduced from the saturation magnetization at low temperatures. Even if the closeness of this comparison is somewhat fortuitous, it still remains that the $n_0$ values at $T_c$ deduced for $S=1$ and $S=\infty$ are in much worse agreement with the low-temperature value. Thus, this quantitative analysis of the susceptibility behavior of nickel near its Curie point strongly favors an $S$ value of $\frac{1}{2}$, suggesting that the electron moments in nickel assume essentially only two orientations (parallel and antiparallel) with respect to each other. A value of $\frac{1}{2}$ for $S$ is also known to be favored by the temperature dependence of the saturation magnetization of nickel

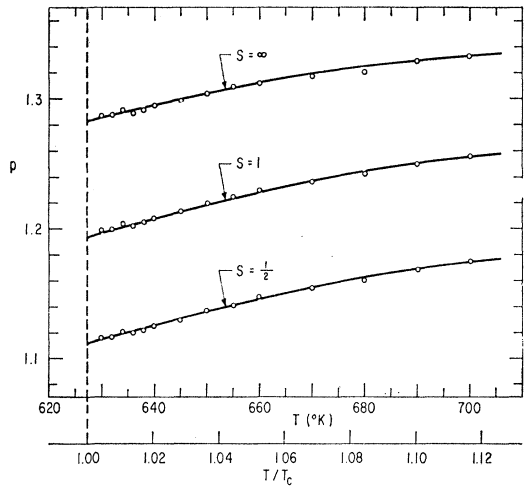


FIG. 5. Temperature dependence of effective paramagnetic moment of nickel obtained from comparison of experimental $\chi_0^{-1}$-versus-$T$ curve with Eq. (6) for different $S$.

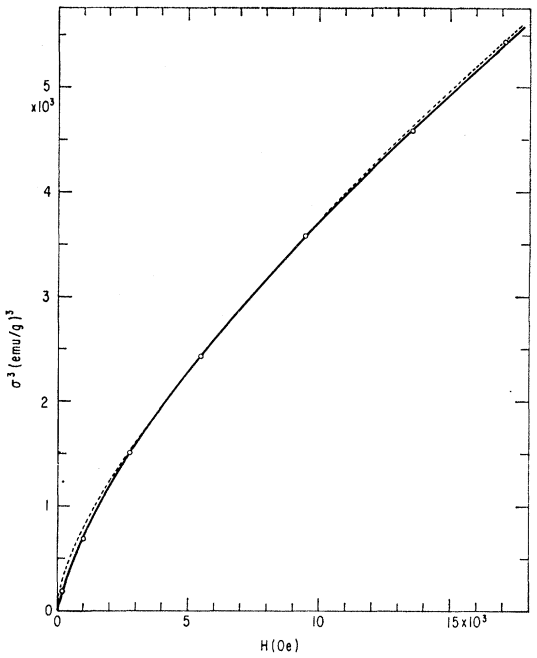


FIG. 6. Magnetization-cubed versus internal field for nickel at its Curie temperature (627.2°K): Solid curve drawn through circled points obtained by interpolation of data in Fig. 1; dotted curve calculated from Eq. (8) for $\epsilon=0.237$.

interpreted on the basis of the molecular-field model[18]; but, as we discussed earlier, this model is unable to explain even qualitatively the properties of nickel near its Curie temperature.

The fact that the inverse susceptibility of nickel just above $T_c$ is found to vary as a simple $(\frac{4}{3})$ power of $T-T_c$ suggests the possibility of an analogously simple relationship at $T_c$ between the magnetization and the field. Since the molecular-field-model expression for this relationship, derivable from Eq. (2a), is

$$\sigma=\sigma_0(q\mu_B H/kT_c)^{\epsilon}, \tag{8}$$

with the exponent $\epsilon$ equal to $\frac{1}{3}$, we consider the possibility that this expression is applicable to nickel at $T_c$, but with $\epsilon$ having some fixed value that is not necessarily $\frac{1}{3}$. By a straightforward interpolation of the Weiss and Forrer data shown in Figs. 1 and 2, we obtain values of magnetization versus internal field for the Curie temperature of 627.2°K. These are shown plotted as $\sigma^3$ versus $H$ in Fig. 6, where the nonlinearity of the curve through the points makes it clear that $\epsilon\neq\frac{1}{3}$ in Eq. (8). The smoothness of this curve, however, allows us to evaluate $d\sigma^3/dH$, as well as $\sigma^3$, at regular intervals of $H$ and then estimate $\epsilon$ from

$$\epsilon=(H/3\sigma^3)d\sigma^3/dH, \tag{9}$$

which follows from Eq. (8). The values of all these quantities are listed in Table III, and it is evident that

[18] See, for instance, Fig. 10–4 in R. M. Bozorth, *Ferromagnetism* (D. Van Nostrand Company, Inc., New York, 1951).

TABLE III. Values of $\sigma^3$ and $d\sigma^3/dH$ obtained at different fields from interpolated $\sigma$-versus-$H$ data for nickel at $T_c$ (=627.2°K), and corresponding values of $\epsilon$ computed from Eq. (9).

| $H$[a] | $\sigma^3$ [b] | $d\sigma^3/dH$[a,b] | $\epsilon$ |
|---|---|---|---|
| 2000 | 1190 | 0.433 | 0.243 |
| 4000 | 1940 | 0.345 | 0.237 |
| 6000 | 2590 | 0.307 | 0.237 |
| 8000 | 3170 | 0.281 | 0.236 |
| 10 000 | 3710 | 0.262 | 0.235 |
| 12 000 | 4210 | 0.247 | 0.235 |
| 14 000 | 4690 | 0.237 | 0.236 |
| 16 000 | 5170 | 0.231 | 0.238 |

[a] $H$ in Oe.
[b] $\sigma$ in emu/g.

the computed $\epsilon$ values are remarkably constant (at about 0.237) over this entire field range. Hence, we are able to achieve a very good approximation to the experimental curve in Fig. 6 with a curve (shown dotted) computed from Eq. (8) with $\epsilon$ fixed at 0.237. The proper scaling of this computed curve was attained by setting $\sigma_0=57.5$ emu/g (i.e., $n_0=0.606$) and $q=3.63$, and we note that this $q$ value, though larger than those listed in Table I for $n_0=0.606$ and different values of $S$, is considerably smaller than the value of 10 deduced earlier (see Fig. 2) from a molecular-field-model interpretation of the data. Alternatively, noting that $\sigma_0$ and $q$ are both proportional to $n_0$, we can solve for $n_0$ by applying Eq. (8) with $\epsilon=0.237$ to the dotted curve in Fig. 6. We thus find for the case of $S=\frac{1}{2}$ that $n_0=0.693$, which is remarkably consistent, considering the empirical status of Eq. (8), with the $n_0$ value of 0.642 that we deduced earlier from the susceptibility behavior near the Curie point.

Unfortunately, there is as yet no firm theoretical prediction for the field dependence of the magnetization of an Ising or Heisenberg ferromagnet at its Curie point. In order to get an experimental basis of comparison for our present results for nickel, we may draw on the analogy between the behavior of a ferromagnet near its Curie point and that of a gas near its critical point.[19] Of particular relevance here is the fact that the field on a ferromagnet and its magnetization are isomorphic, respectively, to the pressure $p$ on a gas and its density $\rho$, where $p$ and $\rho$ are measured with respect to their critical values $p_c$ and $\rho_c$.[20] From a careful analysis of pressure-volume-temperature data on xenon, carbon dioxide, and hydrogen, Widom and Rice[21] were able to show that $|\rho-\rho_c| \propto |p-p_c|^{\epsilon'}$, with $\epsilon'\approx 0.24$ for Xe and $H_2$ and $\epsilon'\approx 0.25$ for $CO_2$. Hence, these results appear to be closely parallel to the magnetization-field relationship in nickel at its Curie point, which we find obeys Eq. (8) with $\epsilon=0.237$.

[19] T. D. Lee and C. N. Yang, Phys. Rev. **87**, 410 (1952); J. W. Essam and M. E. Fisher, J. Chem. Phys. **38**, 802 (1963); M. E. Fisher, J. Math. Phys. **5**, 944 (1964).

[20] More correctly, the magnetic field is isomorphic to the chemical potential of a gas, but this varies linearly with pressure for small changes at the critical temperature (see Ref. 19).

[21] B. Widom and O. K. Rice, J. Chem. Phys. **23**, 1250 (1955).

## SUMMARY

Two features of the magnetic behavior of nickel have been investigated: the temperature dependence of the initial susceptibility $\chi_0$ above the Curie point $T_c$ and the field dependence of the magnetization $\sigma$ at $T_c$. Both these properties, as deduced from a $\sigma^2$-versus-$H/\sigma$ plot of the Weiss and Forrer data, are at variance with the simple molecular-field model. Instead of being linear, the experimental $\chi_0^{-1}$-versus-$T$ curve immediately above $T_c$ is shown to follow the simple relation, $\chi_0^{-1} \propto (T-T_c)^{\gamma}$, with $\gamma=1.35(\pm 0.02)$, in excellent agreement with the $\frac{4}{3}$-power relation recently predicted from exact Heisenberg-model calculations.

Moreover, from the coefficient of proportionality between $\chi_0^{-1}$ and $(T-T_c)^{\gamma}$ at $T_c$, it is deduced that $\mu_0$, the average moment per atom, is $0.642\mu_B$, which agrees closely with the low-temperature value of $0.606\mu_B$, and that the individual electron moments assume essentially only parallel or antiparallel orientations with respect to each other, corresponding to $S=\frac{1}{2}$. At higher temperatures, the experimental $\chi_0^{-1}$-versus-$T$ curve is found to diverge from the Heisenberg-model predictions, and this divergence might be attributable to a gradual rise in $\mu_0$ with increasing temperature.

Up to the highest field of measurement, the magnetization at $T_c$ is shown to vary as $H^{\epsilon}$ with $\epsilon=0.237$. This $\epsilon$ value differs from the value $\frac{1}{3}$ predicted from molecular-field theory but is consistent with the exponent values for an analogous empirical relationship between the density and pressure of several different gases at their critical points.